Accepted Manuscript

Intramolecular interactions, isomerization and vibrational frequencies of two paracetamol analogues: A spectroscopic and a computational approach

Rommel B. Viana, Gabriela L.O. Ribeiro, Sinara F.F. Santos, David E. Quintero, Anderson B. Viana, Albérico B.F. da Silva, Rodolfo Moreno-Fuquen

Intramolecular interactions, isomerization and vibrational frequencies of two paracetamol analogues: a spectroscopic and a computational approach

Rommel B. Viana [1*], Gabriela L.O. Ribeiro [1], Sinara F.F. Santos [1], David E. Quintero [1],

Anderson B. Viana [2], Albérico B.F. da Silva [1], Rodolfo Moreno-Fuquen [3]

1. Instituto de Química de São Carlos, Universidade de São Paulo, São Carlos-SP, Brazil.

2. Departamento de Engenharia Oceânica, Centro de Tecnologia, Instituto Alberto Luiz Coimbra de Pós Graduação e Pesquisa de Engenharia (COPPE), Universidade Federal do Rio de Janeiro, Rio de Janeiro-RJ, Brazil.

3. Departamento de Química, Facultad de Ciencias, Universidad del Valle, Santiago de Cali, Colombia.

[*]Corresponding authors.
Email: rommelbv@yahoo.com.br

Av. Trabalhador São Carlense, 400 (caixa-postal: 780). Bairro: Centro. CEP: 13560970 - São Carlos, SP – Brazil.

-2-

ABSTRACT

The aim of this investigation was to determine the molecular properties and provide an interpretation of the vibrational mode couplings of these two paracetamol analogues: 2-bromo-2-methyl-N-(4-nitrophenyl)-propanamide and 2-bromo-2-methyl-N-p-tolyl-propanamide. E/Z isomers, keto/enol unimolecular rearrangement and prediction of the transition state structures in each mechanism were also assessed using the Density Functional Theory (DFT). The DFT estimates a high energy gap between E and Z isomers (9-11 kcal·mol^{-1}), with barrier heights ranging from 16 to 19 kcal·mol^{-1}. In contrast, the barrier energies on the keto/enol isomerization are almost 10 kcal·mol^{-1} higher than those estimated for the E/Z rearrangement. The kinetic rate constant was also determined for each reaction mechanism. Natural bond orbital analysis and the quantum theory of atoms in molecules were used to interpret the intramolecular hydrogen bonds and to understand the most important interactions that govern the stabilization of each isomer. Furthermore, an analysis of the atomic charge distribution using different population methodologies was also performed.

INTRODUCTION

Paracetamol is considered to be a first-line treatment for children's pain and fever because of its analgesic and antipyretic actions [1]. Because of the different environmental [2-5] and pharmacological implications of paracetamol [6-10], several investigations have been performed to assess its spectroscopic properties [11-15] and to determine the different aspects of its crystallization [16-21]. Different paracetamol derivatives have also been shown to have antioxidant activity [22,23] as a fatty acid amide hydrolase inhibitor [24], and these derivatives are potentially safer analgesics than paracetamol itself [25-32].

The purpose of this study is to describe the electronic properties and provide an interpretation of the vibrational mode couplings in these two paracetamol analogues: 2-bromo-2-methyl-N-(4-nitrophenyl)-propanamide and 2-bromo-2-methyl-N-p-tolyl-propanamide (Figure 1). In this investigation, we will characterize the E/Z isomers, the keto/enol unimolecular arrangement and the transition state structures in each mechanism. A Natural Bond Orbital (NBO) analysis and a topological analysis using the Quantum Theory of Atoms in Molecules (QTAIM) [33] will also be performed. These compounds have already been synthesized and their structures were analyzed using X-ray diffraction [34,35]. However, there are few studies on their electronic properties and also little information on the details of their vibrational frequencies and their respective vibrational couplings. Therefore, a combined experimental and quantum chemical investigation on the electronic properties will provide a good understanding of these systems, as shown in previous studies [36-42].

MATERIALS AND METHODS

The compounds were synthesized using the procedure published by Moreno-Fuquen *et al.* [34,35]. The infrared spectrum was recorded between KBr windows from 4000 to 400 cm^{-1} on a FTIR GX1 spectrophotometer with a resolution of 1 cm^{-1} and using 64 scans.

All the calculations were carried out using the GAUSSIAN 09 program [43]. Stationary points on the potential energy surface were fully optimized, and harmonic vibration frequencies were evaluated to characterize their nature as minima. The absence of imaginary frequencies indicated that all optimized structures were the true minimum. The PBE1PBE functional [44,45] was used in the optimization procedure with the 6-31G(2df,2pd) basis set [46,47]. A tight convergence and an *ultrafine* grid were used in the optimization procedure. The PBE1PBE functional demonstrated a good performance in to estimate the electric dipole moment and polarizability [48] as well as in to the prediction of the transition state structures in organic reactions [49,50] and in unimolecular rearrangements [51]. The transition state structures (TSs) were searched using the synchronous transit-guided quasi-Newton method [52,53], where is required the reactant and product for the structure as input. The TS structures were then optimized with analytical gradients using the Berny algorithm with redundant internal coordinates until a stationary point on the potential surface was found. Finally, the transition state structures were verified by subsequent frequency calculations, which allowed us to determine the imaginary vibrational frequencies related to the reaction path. A Hessian-based predictor-corrector reaction path algorithm [54,55] was also used to confirm the reactant and the product of each TS structure. In addition, M05-2X [56] and BMK [57] functionals were also applied in the energetic profiles of the reaction pathways due to their accurate prediction of chemical reaction barrier heights for modeling kinetic

rate constants [56-59]. For these both DFT functionals were employed the 6-311++G(d,p) basis sets [46,47]. All simulations were performed in gas phase

The atomic charge analysis was performed using different methodologies: Mulliken, Lowdin, generalized atomic polar tensor (GAPT) [60], Natural Population Analysis (NPA) [61], Chelp [62], ChelpG [63], Merz-Singh-Kollman (MK) [64,65] and the Hirschfeld method [66,67]. NBO analysis was performed using the NBO 6.0 program [68]. Topological analysis with QTAIM was performed using the AIMALL program [69]. In the charge analysis, bond indexes, NBO and QTAIM calculations were used the PBE1PBE/6-31G(2df,2pd) method.

RESULTS AND DISCUSSION

Geometry and structure prediction

The structure prediction showed good agreement between the experimental and PBE1PBE/6-311G(2df,2pd) geometry, mainly when the bond lengths and angles were compared. The mean absolute error (MAE) for **c1** and **n1** were 44% and 55%, respectively. Nevertheless, the MAE values is around 6% when compared the experimental and calculated bond lengths, while these values decreases to 1% examining the bond angles. The main reason for this difference is likely a result of the quantum chemical calculations where the molecules were simulated in vacuum. However, X-ray analysis was performed on a single-crystal sample and the crystal packing was shown to affect the structure geometry. We compared the experimental and the predicted dihedral angles. For **c1**, the C_{11}-N_{13}-C_6-C_1 torsional angle was -31.2(5)° as shown using X-ray analysis [35], while with the PBE1PBE functional is 0.2°. For **n1**, the experimental [34] and predicted C_{11}-N_{13}-C_6-C_1 angles were 12.7(4)° and 0.0°, respectively. The large value for the **c1** C_{11}-N_{13}-C_6-C_1

torsional angle occurs because this molecule is stabilized by three intermolecular interactions that are formed by each carboxyl group (a NH-O hydrogen bond and two weak CH-O bonds). In contrast, **n1** presents two intermolecular interactions for each amide group: a CH-O and a NH-O hydrogen bond [34]. Another example of a dihedral angle that is affected by the crystal packing is the Br-C_{12}-C_{11}-O_{15} angle. In **c1**, the Br-C_{12}-C_{11}-O_{15} experimental torsional angle is -100.5(3)°, while it was estimated to be 179.9° using the PBE1PBE/6-311G(2df,2pd) method. For **n1**, the experimental and predicted Br-C_{12}-C_{11}-O_{15} angles are -97.1(2)° and 180°, respectively.

Frontier orbitals, atomic charge distribution and heat of formation

Figure 2 shows the highest occupied molecular orbital (HOMO) and lowest unoccupied molecular orbital (LUMO) in paracetamol and their analogues investigated here. The main contribution for **c1** and **n1** HOMOs come from the bromine lone-pair electrons [$_{lp}$(Br)], with a minor contribution from the σ_{CC} bonds and a very small contribution from the lone-pair electrons from nitrogen [($_{lp}$(N)] and oxygen atoms [$_{lp}$(O)]. In contrast, for paracetamol is seen large contribution from aromatic ring in HOMO as well as from σ_{CN} and $_{lp}$(O). The major contribution in the **c1** LUMO comes from anti-bonding π_{CC} (π^*_{CC}), while in **n1**, there is also a contribution from the σ_{CN} bond and from the $_{lp}$(O) of the NO_2 group, as well as from the σ^*_{CN} of the amide group. Examining the HOMO-LUMO gap of paracetamol and their analogues is seen only a small difference among these structures, where the largest value is estimated from **n1**. This difference in the **n1** HOMO-LUMO energy gap occurs mostly in response to the large stabilization of its LUMO that results from the change in the substituent group that increases the **n1** electron-acceptor character.

Another important issue is a population analysis of the atomic charge distribution (see ST1, in the supplementary material). Examining the QTAIM charge distribution, we found that a larger negative charge is estimated for the oxygen of the carbonyl group $[q(O)_{CO}]$ than for the bromine charge $[q(Br)]$, while the largest positive charge is estimated for the carbon atom in the carbonyl group $[q(O)_{CO}]$. In addition, we used different methodologies to evaluate the susceptibility of the partial atomic charge distribution that results from the population method that was used, including the Mulliken, Lowdin, GAPT, NPA, Chelp, ChelpG, MK and the Hirschfeld methods. The QTAIM charge was used as the reference value because this charge framework is obtained by the integration of electronic density within the atomic basis followed by addition of the nuclear charges [33], making the QTAIM methodology the most reliable option. Although the QTAIM method led to a high separation between the element charges (particularly because of its partition scheme), the QTAIM methodology showed good efficiency compared to other population methods, which has also been confirmed for other systems [70-74]. The ChelpG, GAPT, Mulliken and MK methods showed small differences from the QTAIM values and all the methodologies showed a good efficiency to predict the partial atomic charge distribution, with the exception of the Lowdin charge. This lowest performance of Löwdin charges is due to this population method does not lead to good results as the basis set is increased for a triple zeta quality and the values may behave unpredictably [75]. Specific examples were the bromine charge and the $-CH_3$ and $-NO_2$ peripheral groups. The NPA and the Lowdin charge showed a large difference from the QTAIM value in the bromine charge, while only the Mulliken, GAPT and Hirschfeld methods predicted the correct sign for $q(Br)$. For the $-CH_3$ and $-NO_2$ peripheral groups, only the GAPT method estimated the correct character for both groups. Therefore, based in these results, it is noteworthy to mention that QTAIM

and GAPT method are the most appropriate population methods to analysis the paracetamol analogues.

To provide more information about of the two paracetamol derivatives, we also estimated the heat of formation at 0K and 298K. It is important to address that the heat of formation is an important energy descriptor parameter in the quantitative structure-activity relationships (QSAR) for drug design with the objective to capture complex relations between relevant descriptors in order to evaluate the biologic activity of different molecules [76-78]. The methodology proposed by Curtis *et al.* [79] was used to calculate the heat of formation, which combines *ab initio* and experimental values. The experimental heat of formation at 0 K for the elements was provided by NIST-JANAF [80] for the total atomization energy, as follows: C (ΔH_f^{0K}=171.29 kcal·mol^{-1}), N (ΔH_f^{0K}=112.97 kcal·mol^{-1}), O (ΔH_f^{0K}=59.55 kcal·mol^{-1}), H (ΔH_f^{0K}=51.63 kcal·mol^{-1}) and Br (ΔH_f^{0K}=26.74 kcal·mol^{-1}). The carbon (-0.08 kcal·mol^{-1}), oxygen (-0.22 kcal·mol^{-1}) and bromine (-3.51 kcal·mol^{-1}) spin-orbit corrections were obtained according to Moore [81]. These calculations were carried out using the G3MP2 method [82]. The **c1** heat of formation at 0K was -24.26 kcal·mol^{-1}, while that of **n1** was -21.61 kcal·mol^{-1}. In addition, at 298K, the heat of formation for **c1** and **n1** was -34.66 and -32.10 kcal·mol^{-1}, respectively.

Relative stability among the isomers, transition state structures and rate constants

The relative stability and the electric dipole moment among the different positions of functional groups in the phenyl ring (**A**-**E** isomers) can be seen in Figure 3. In **c1** regioisomers, it can be noted that the different positions of methyl groups caused only a small effect in the electric dipole moment. However, the electric dipole moment ranged from 2.6 to 6.5 Debye considering the **n1** regioisomers. In terms of the energetics, isomer **B** demonstrated the largest energy gap for both

paracetamol analogues. Among **c1** regioisomers, isomers **C-E** presented an energy difference lower than 0.5 kcal mol^{-1} when compared with isomer **A**. In **n1** regioisomers, the relative stability analysis confirmed isomer **A** as the most stable conformation, while the energy difference from isomers **C-E** varied from 0.7 to 2.7 kcal mol^{-1}.

The relative stability of the two paracetamol analogues is shown in Figure 4. The *E*/*Z* reactions are slight exoergic, and the energy gap between **c1** and **c2** ranged from 9.6 to 10.5 kcal·mol^{-1}, demonstrating only a slight increase in the *E*/*Z* energy difference that results from the NO$_2$- substitution. These results are also in good agreement with the values predicted by Aydin *et al*. [83] for a pyrimidine derivative. An important aspect in Figure 3 is the transition state structure **TS1**, which connects the *E* and *Z* isomers. For **TS1c**, barrier height is estimated to have an energy of 9.6 kcal·mol^{-1} with PBE1PBE and M05-2X functionals and an increase of 1 kcal·mol^{-1} was found using the BMK functional. In contrast, the barrier energy increases almost 1 kcal·mol^{-1} for **TS1n**, with the PBE1PBE functional. It is noteworthy to comment that these barrier energies were smaller than what was predicted by Sargol *et al*. for an acyl hydrazone derivative [84]. Sargol and co-authors estimated the barrier heights at 18 kcal mol^{-1} for the E/Z unimolecular rearrangement, but the *E*/*Z* energy gaps were smaller than 1 kcal·mol^{-1}.

On the other hand, the keto/enol energy difference varied between 16 and 19 kcal·mol^{-1} for both paracetamol analogues. **TS2** represents the transition state structures that connect the *Z* isomers with the enol configurations, where the reaction pathway is carried out by a proton transfer from the amine group into the keto functional group, which leads to formation of the enol group. The barrier at **TS2c** is 37 kcal·mol^{-1} relative to **c2** with M05-2X and BMK functional, while the **n2→n3** reaction also shows a sizable entrance barrier, varying from 32.6 to 37.3 kcal·mol^{-1}. Note that

reverse routes involve barriers of 25-30 kcal·mol^{-1} with a small difference between both paracetamol analogues.

We also predicted the Gibbs free energy and the rate constants for each process at 298K (Table 1). We used the canonical transition state theory to calculate the rate constants. We can see that the E/Z isomerization pathways ranges from 2.58×10^{-2} to 1.46 s^{-1}. These reactions also show small half-lives where the highest value (39 seconds) was predicted for the **c1→TS1c→c2** reaction using the PBE1PBE functional. The reverse route (**c2→TS1c→c1**) half-life is estimated to be less than 4 ns, while this same process increases two orders of magnitude for the NO_2 analogue. On the other hand, the rate constants in the keto/enol pathways varied from 4×10^{-15} to 6×10^{-12} s^{-1} because of the large Gibbs free energy of activation, and these half-lives ranged from 10^{11} to 10^{14} s. In contrast, the reverse route is five orders of magnitude faster considering the M05-2X/6-311++G(d,p) method.

Molecular electrostatic potentials, bond order indices, NBO analysis and other different properties of each isomer

Further insights into the electronic structure of the paracetamol analogues can be obtained when the electric dipole moment is analyzed (Table 2). A look at nitro isomers shows that the electric dipole moment increases in the following order: **n2**<**n1**<**n3**. However, the difference between the **n1** and **n3** dipole moment is less than 4%. In contrast, the dipole moment of the isomers with the methyl group can be arranged in the following order: **c1**<**c3**<**c2**. In this case, the **c2** dipole moment is 70% larger than that of **c1**. We also performed a QTAIM analysis between methyl isomers to determine the main reason for this difference in the dipole moment. An inspection of the **c1→c2** configuration change reveals an increase in the contribution of the

formamide group followed by a decrease of the $C(CH_3)_2Br$ group, and a slight increase in the *p*-tolyl contribution is also noted. According to the polarizability, the difference among the isomers is larger among the CH_3- species than among NO_2- isomers.

Another important property is the octanol/water partition coefficient (log P), which measures the hydrophobicity of the compounds (see Table 2). Log P was calculated according to Ghose *et al.*'s atom fragment method [85] that was implemented in the Hyperchem program [86], which has been used with success to predict experimental values [87-90]. Generally, log P<0 indicates a hydrophilic nature for the compound, while a lipophilic and an amphiphlic character is expected when the result is log P>1.5 and 0<log P<1.5, respectively. For the paracetamol isomers that are estimated to have a lipophilic character, a decrease of log P for enol configurations is predicted. Using the surface area and the volume of each isomer, the lowest values for *Z* configurations can be estimated, and these results are similar to those of the enol species. Moreover, the refractive index difference among the CH_3- and NO_2- isomers is less than 5%.

The nitrogen-oxygen bond order index among the isomers was also studied (see ST2 in the supplementary material). The Mayer bond index [91] was used in the E/Z configuration change, and we estimated an increase in the C-N bond order (from 1.0 to 1.2), followed by a slight increase in the C=O bond order value (from 1.9 to 2.0). Nevertheless, an increase in the C-N bond order to 1.9 is predicted after the keto/enol isomerization, which occurs because the bond character changes from a σ bond to a π bond. This bond nature change is also seen for the C-OH bond, where the Mayer bond index changes from 2.0 to 1.2. In contrast, the σ C-Br bond order values do not show significant changes for each reaction.

To evaluate the susceptibility of the bond index methodology, the Wiberg bond index (bo_{wi}) [92], the bond delocalization index (BDI) [93] and the atom-atom overlap natural localized

molecular orbitals/natural population analysis bond index (bo_{nlmo}) [94] were also used. An interesting case is the C-N bond in the formamide group on the **c1**→**c2** isomerization, where the Mayer index and bo_{nlmo} predicted an increase in the bond order, while the Wiberg index estimated a decrease in bond order. BDI did not show any significant change in the bond order value (less than 2%). In contrast, the nitro analogue reaction was different. In the **n1**→**n2** configuration change, only BDI and bo_{nlmo} showed any significant change in the C-N bond order (less than 3%), while the Mayer and Wiberg bond indices predicted small increases in the bond order value of 9% and 5%, respectively.

Figure 4 presents the molecular electrostatic potential map of each isomer. In the electrostatic potential maps, the positive regions (in blue) refer to areas where the nucleophilic character is estimated, while the red areas are the areas that demonstrate an electrophilic nature and green represents the neutral regions. Among the isomers, the main electrophilic regions are presented in the phenyl ring and in carbonyl group, but a decrease in the electrophilic regions in the Z isomers is estimated. Among the isomers, the differences that are caused by CH_3- and NO_2-substituent groups are also important. In isomers with nitro functional groups, there is a decrease in the phenyl electrophilic character, particularly because of the charge transfer to the NO_2- group. This issue became clearer when we compared **c2** and **n2** electrostatic potential maps. In **c2**, the main electrophilic areas were localized in the phenyl ring and in the carbonyl group, while in **n2**, these areas are in the carbonyl and nitro group.

NBO calculations estimate that the electrostatic effect is predominant in **c3**, while the steric effects are predominant in **n3**. In **n2**, the steric repulsion and the electrostatic effect have a similar contribution, although very small. Similar characteristics are seen for **c2**, but the electrostatic effects are two times higher than the steric contribution. Moreover, we also performed a second order

perturbation theory analysis of a Fock matrix based on the NBO. Analyzing the interaction between nitrogen lone pairs $[l_p(N)]$ and σ_{CO} antibonding (σ^*_{CO}) $[l_p(N)\rightarrow\sigma^*_{CO}]$ showed a decrease of 16 kcal·mol^{-1} in the E/Z unimolecular rearrangement based on the second-order interaction energy (E^2). In addition, in the **c1→c2** reaction, the charge transfer from $l_p(N)$ into aromatic π^*_{CC} $[l_p(N)\rightarrow\pi^*_{CC(arom)}]$ decreased by 13 kcal·mol^{-1}, while the $\pi_{CC(arom)}\rightarrow\pi^*_{CC(arom)}$ charge transfer showed an estimated increase of 10 kcal·mol^{-1}. In the **n1→n2** reaction, the decrease in the $l_p(N)\rightarrow\pi^*_{CC(arom)}$ interaction is less than 3 kcal·mol^{-1}, while the $\pi_{CC(arom)}\rightarrow\pi^*_{CC(arom)}$ donation decreased by 12 kcal·mol^{-1}. The $l_p(O)\rightarrow\sigma^*_{CN}$ and $l_p(O)\rightarrow\sigma^*_{CC}$ interaction is also important, but the E^2 energy decrease was small. For the **c2→c3** reaction, an energy decrease of 49 kcal·mol^{-1} is predicted in the $l_p(N)\rightarrow\sigma^*_{CO}$ interaction, and also reveals an increase of 21 kcal·mol^{-1} in the $l_p(N)\rightarrow\pi^*_{CC(arom)}$ donation.

QTAIM analysis of intramolecular interactions

Figure 5 shows the molecular graphics of each isomer, indicating the bond paths, bond critical points (BCPs, in green), the ring critical points (RCPs, in red) and the cage critical points (CCPs, in blue). QTAIM analysis was performed on several parameters (Table 3) such as the electronic charge density $[\rho(r)]$ and its Laplacian $[\nabla^2\rho(r)]$, the total energy density $[H(r)]$, the ellipticity (ε) and the relationship between the modulus of the local potential energy and the local energy density $[|V(r)|/G(r)]$. Thus, shared interaction (in most of the covalent compounds) shows large electron densities, which are followed by negative values in its Laplacian, while closed-shell interactions present low $\rho(r)$ values and positive $\nabla^2\rho(r)$ values that are associated with their ionic nature or van der Waals compounds [95]. The *E* isomers have two BCP associate intramolecular interactions: the O-HC and Br-HN interactions. The electronic charge density of the **c1** and **n1** O-

-14-

HC interactions are 0.01851 and 0.01935 a.u., respectively, while that of the Br-HN interactions are also similar (0.024 a.u.). The $\nabla^2\rho(r)$ results for both interactions show positive values, indicating the ionic nature in these two interactions.

Another important parameter is the electronic energy density found by Cremer and Kraka [96], which is the sum of the local kinetic and potential energy density at the BCP. When H(r) is negative, this indicates a stabilization in the accumulation of electronic charge in the internuclear region (a characteristic of a covalent interaction), while a positive result shows that the accumulation of electronic charge leads to a destabilization of the system, which is a characteristic of van der Waals and ionic bonding systems. The H(r) results for the O-HC interactions are positive, emphasizing their ionic character in *E* isomers. The Br-HN total energy density between *E* isomers shows a more negative value for the **n1** H(r), which suggests a large electronic charge concentration between the Br and H basins. The H(r) values show different characteristics between the **c1** and **n1** Br-HN interaction [a positive (6×10^{-5} a.u.) and a negative (-1×10^{-4} a.u.) value, respectively], both resulting in a very small interaction, which does not imply a distinguishing nature for each interaction and also emphasizes their ionic nature.

The covalent nature of each interaction can also be analyzed when we take into account the |V(r)|/G(r) relationship, where this ratio may work as an estimation of the "covalence" character of a bonding interaction. A |V(r)|/G(r) relationship greater than 2, indicates a covalent interaction, a value smaller than 1 indicates a noncovalent interaction and a value between 1 and 2 indicates a partially covalent interaction. Examination of the O-HC interaction in the *E* isomers revealed a |V(r)|/G(r) value less than 1, demonstrating their noncovalent character; this relationship indicates a partial covalent nature for the Br-HN interactions. Another important aspect is the ellipticity, which can work as an indicator of the instability in each interaction. Ellipticity shows a higher value for

the O-HC interaction than for the Br-HN interaction, which suggests that the Br-HN interaction is more stable than the O-HC interaction.

We further studied the intramolecular interactions among the other isomers. Analysis of the Z isomers and enol species showed two intramolecular interactions: Br-HC and CH-C. An interesting parameter in CH-C interactions is the large ellipticity value, which confirms the instability of these intramolecular interactions and their ionic character when the $|V(r)|/G(r)$ relationships are investigated. On the other hand, comparing the ellipticity results in Br-HC interactions between both Z isomers shows a value an order of magnitude lower for **n2**, which reveals its higher stability. Moreover, a distinguishing characteristic in **n2** is the presence of a CCP. In this CCP, the electronic density is lower than in the other three surrounding RCPs, while an examination of the kinetic energy density shows that the electrons move similarly in CCP and RCPs.

Vibrational spectral analysis

In this section, we will discuss the infrared characteristic bands of the two paracetamol analogues and their assignments, based on a comparison between the simulated spectra in a vacuum and experimental spectra in the solid state. The discussion in this section only involves **c1** and **n1** infrared vibrational frequencies. The experimental FT-IR spectrum of **c1** and **n1** are presented in Figures 6 and 7, respectively. The vibrational wavenumber assignments were performed through visualization of vector displacement in the AVOGRADO [97] program, but for this task we did not use any scale factor.

Carbon-Bromine and NO$_2$ vibrational modes

For a compound with a NO$_2$ group, the symmetric [$\nu(NO_2)_{as}$] and asymmetric [$\nu(NO_2)_{sym}$] stretching vibrational modes are usually located in the regions 1540-1625 cm^{-1} and 1360-1460 cm^{-1}, respectively [98,99]. In the **n1** infrared spectrum, the $\nu(NO_2)_{sym}$ and $\nu(NO_2)_{as}$ are localized at 1340 and 1528 cm^{-1}, respectively. The NO$_2$ scissoring band is detected at 855 and 751 cm^{-1} in the FT-IR spectrum. In addition, the deformation vibrations of the NO$_2$ group as rocking and wagging modes are in the low frequency region [98,99].

Carbon-halogen vibration frequencies are assigned in a wide frequency range of 480-1129 cm^{-1}, based on previous reports [98,99], because these bands are highly affected by adjacent atoms or groups. For example, the C-Br stretching [$\nu(C-Br)$] band is observed at the 700-1070 cm^{-1} region in bromine-phenyl groups [100-103], but this band is detected at 481 cm^{-1} in p-bromonitrobenzene [104] and at 540 cm^{-1} in α-bromotoluene [105], demonstrating the effect of peripheral groups. In the **c1** FT-IR spectrum, the $\nu(C-Br)$ band is observed at 696 cm^{-1}, and also has 2 shoulders at 650 and 628 cm^{-1}. The shoulder at 650 cm^{-1} is associated with the N-H wagging mode, while the shoulder at 628 cm^{-1} is a result of the $\nu(C-Br)$ mode coupled with the C-H out-of-plane vibrations. Based on DFT calculations, the $\nu(C-Br)$ peak was predicted at 692 cm^{-1}, and the two shoulders are estimated at 656 and 646 cm^{-1}. In the **n1** infrared spectrum, there is a band that is divided into two peaks at 692 and 673 cm^{-1} with small bandwidths. The frequency at 692 cm^{-1} is assigned to the $\nu(C-Br)$ vibration and the band at 673 cm^{-1} is a result of the N-H wagging mode.

Carbon-Hydrogen and Carbon-Carbon vibrational modes

The fundamental CH$_3$ bands are usually detected in the region between 2950 and 2990 cm^{-1} [92,93]. In **n1**, the symmetric CH$_3$ [$\nu(CH_3)_{sym}$] vibrational mode is detected at 2930 cm^{-1}. In the **c1**

FT-IR spectrum, the band at 2857 cm^{-1} is assigned to $\nu(CH_3)_{sym}$ of the methyl-phenyl group, while the peak at 2923 cm^{-1} is related to the $\nu(CH_3)_{sym}$ modes in the $C(CH_3)_2Br$ peripheral group. These results are in agreement with previous studies [106-109]. In addition, the asymmetric CH_3 [$\nu(CH_3)_{as}$] frequency in the **n1** infrared spectrum showed a band at 2978 cm^{-1} with a shoulder at 3005 cm^{-1}. Conversely, in **c1**, the peak at 2983 cm^{-1} is associated with the $\nu(CH_3)_{as}$ mode of the methyl-phenyl group, and the bands at 3005 and 3036 cm^{-1} are assigned to the $\nu(CH_3)_{as}$ frequency of the $C(CH_3)_2Br$ group. For CH_3 vibrational modes in **c1**, these two well-separated peaks for the $C(CH_3)_2Br$ peripheral group are a result of the CH-O intermolecular interactions in the crystal packing.

The aromatic C-H stretching vibrations occurs in the region of 3100-3000 cm^{-1} [98,99]. In **c1**, the experimental C-H aromatic peaks are observed at 3127-3060 cm^{-1}, while this region was estimated in the range of 3262-3171 cm^{-1} using the PBE1PBE functional. The aromatic bands in **n1** were detected in the region of 3134-3049 cm^{-1}, and when we performed the DFT simulations, shifted values for **c1** that resulted from the simulations performed in a vacuum were predicted in this region (in 3269-3190 cm^{-1}).

For the C-H in-plane and out-of-plane bending vibrations in the phenyl ring, both modes usually lie in the regions 1500-1350 cm^{-1} and 1000-600 cm^{-1}, respectively [98,99]. The strong bands at 1471, 1404 and 1369 cm^{-1} in the infrared spectrum corresponds to **c1** C-H in-plane bending vibration modes, while DFT frequencies were predicted in 1455, 1490 and 1590 cm^{-1}. In **n1**, C-H in-plane bending modes were detected as small intensities at 1406 and 1373 cm^{-1} in the experimental FT-IR spectrum, while the C-H out-of-plane bending vibrations were observed at 882 and 830 cm^{-1}, which shows similar values as those of the DFT frequencies (in 900 and 853 cm^{-1}). In

addition, C-H out-of-plane bending bands occur at 813, 893 and 942 cm^{-1} in the **c1** FT-IR spectrum, while these modes were estimated at 838, 952 and 985 cm^{-1} using the DFT simulation.

Vibrational modes associated with the amide group

The N-H stretching [ν(N-H)] band shows a strong signal in both infrared spectra. In **c1**, the ν(N-H) mode appears as a strong and broad band in the region of 3156-3416 cm^{-1}, with a maximum intensity localized at 3303 cm^{-1}. This result is similar to previous studies [110-112]. The DFT results showed a blue-shift of 288 cm^{-1} when we compared with the **c1** ν(N-H) experimental value. The ν(N-H) band in **n1** appears as a tight peak at 3407 cm^{-1}, which is in agreement with results from Kolev *et al*. [113] for a butenoic-phenylamide structure. In addition, a blue-shift of 168 cm^{-1} was also seen compared with the experimental results with the **n1** simulated value. An explanation for this difference in the shape of the ν(N-H) band between these molecules may be a result of the **c1** crystal packing that is stabilized by three intermolecular interactions formed by each carboxyl group, while in **n1**, there is a CH-O and a NH-O hydrogen bond for each amide group.

The carbonyl stretching frequencies [ν(C=O)] are expected in the region 1680-1715 cm^{-1} [98,99], and those for **n1** and **c1** are detected at 1701 and 1657 cm^{-1}, respectively. For this vibrational mode, there is also a tight band for **n1**, while the ν(C=O) band shows a broad shape for **c1**, particularly because the hydrogen bonds in the crystal packing. Using the PBE1PBE functional, these peaks are predicted at 1797 and 1787 cm^{-1} for **n1** and **c1**, respectively, while the **c1** ν(C=O) intensity is almost two times higher than the estimated intensity in **n1**. The **c1** result is also in good agreement with El-Shahawy *et al*. [114], who detected the ν(C=O) mode in 1640 cm^{-1} for paracetamol. Comparing the experimental and predicted ν(C=O) frequencies, the differences in the estimates were higher than previous studies. For example, Panicker *et al*. [110] estimated a blue-

shift of 35 cm^{-1}, Mary *et al*. [112] estimated a blue-shift of 24 cm^{-1} and Kolev and Angelov [113] estimated a blue-shift of 6 cm^{-1}. In this study, we found a shift of 96 cm^{-1} for **n1**, and a blue-shift of 130 cm^{-1} for **c1** when the experimental and DFT ν(C=O) frequency values were compared. In addition, the peak of the amide NH-C=O group occurs at 1600 cm^{-1} at the **c1** FT-IR spectrum, in contrast with the scissoring band in the **n1** spectrum that has two peaks at 1613 and 1597 cm^{-1}, which are caused by hydrogen bonds in the crystal packing.

The C=O in-plane and out-of-plane deformations [98,99] occur in the regions of 625±70 and 540±80 cm^{-1}, respectively. In **c1**, the C=O in-plane deformation is detected at 638 cm^{-1}, and with the PBE1PBE functional, it is predicted at 641 cm^{-1}. The C=O out-of-plane deformation peak is estimated at 486 cm^{-1} for **c1**, while in the FT-IR, it occurs at 499 cm^{-1} with a very small signal. The **n1** C=O in-plane and the out-of-plane deformation bands are localized at 638 and 499 cm^{-1}, respectively, while DFT simulations predicted a blue-shift that is less than 20 cm^{-1} for both vibrational modes. Moreover, the N-H rock in-plane peaks of **c1** and **n1** in FT-IR are observed at 1164 and 1150 cm^{-1}, respectively. Another important peak is the C-N stretching vibration coupled with N-H out-of-plane wagging, which in general is localized in the region 1275±55 cm^{-1} [98,99]. For **c1** and **n1**, this mode occurs at 1320 and 1338 cm^{-1}, respectively.

CONCLUSIONS

This research has provided insight into several properties of two paracetamol analogues: 2-bromo-2-methyl-N-(4-nitrophenyl)-propanamide and 2-bromo-2-methyl-N-p-tolyl-propanamide. The heat of formation for **c1** and **n1** at 298K was -34.66 and -32.10 kcal mol^{-1}, respectively. An atomic charge distribution showed a larger negative charge for the oxygen atom of the carbonyl group compared with the bromine charge, and the largest positive charge is estimated for the carbon atom in the carbonyl group. Of the methodologies that were used, ChelpG, GAPT, Mulliken and MK showed small differences from QTAIM. In addition, the energy gap between *E* and *Z* isomers was

-20-

less than 10 kcal mol^{-1}, while the keto/enol energy difference was almost two times higher. A similar picture is also reported here when the barrier heights are considered. The barrier energies in the E/Z unimolecular rearrangement are two times lower than the barrier heights in the keto/enol isomerization. For the kinetics, the rate constants in E/Z isomerization pathways range from 3×10^{-2} to 1.46 s^{-1}, leading into a half-life of 39 seconds. The rate constants in the keto/enol pathways, however, varied from 10^{-15} to 10^{-12} s^{-1}.

Acknowledgments

REFERENCES

[1] S.T. Duggan, L.J. Scott, Drugs 69 (2009) 101-113. [doi: 10.2165/00003495-200969010-00007]

[2] M. Bedner, W.A. MacCrehan, Environ. Sci. Technol. 40 (2006) 516-522. [doi: 10.1021/es0509073]

[3] J. Lienert, K. Gudel, B.I. Escher, Environ. Sci. Technol. 41 (2007) 4471–4478. [doi: 10.1021/es0627693]

[4] L. Yang, L.E. Yu, M.B. Ray, Environ. Sci. Technol. 43 (2009) 460-465. [doi: 10.1021/es8020099]

[5] S. Chiron, E. Gomez, H. Fenet, Environ. Sci. Technol. 44 (2010) 284–289. [doi: 10.1021/es902129c]

[6] I. Mahe, C. Caulin, J.-F. Bergmann, Drug Safety 27 (2004) 325-333. [doi: 10.2165/00002018-200427050-00004]

[7] D. Kwan, W. R. Bartle, S. E. Walker, J Clin Pharmacol. 39 (1999) 68-75. [doi: 10.1177/00912709922007570]

[8] D. P. Williams, C. Garcia-Allan, G. Hanton, J. L. LeNet, J. P. Provost, P. Brain, R. Walsh, G. I. Johnston, D. A. Smith, B. K. Park, Chem. Res. Toxicol. 17 (2004) 1551-1561. [doi: 10.1021/tx049846x]

[9] A.E. Mutlib, T.C. Goosen, J.N. Bauman, J.A. Williams, S. Kulkarni, S. Kostrubsky, Chem. Res. Toxicol. 19 (2006) 701-709. [doi: 10.1021/tx049846x]

[10] C. Chen, K.W. Krausz, Y.M. Shah, J.R. Idle, F.J. Gonzalez, Chem. Res. Toxicol., 22 (2009) 699-707. [doi: 10.1021/tx800464q]

[11] H. Hojjati, S. Rohani, Org. Process Res. Dev. 10 (2006) 1101-1109. [doi: 10.1021/op060073o]

[12] B. Bojko, A. Sułkowska, M. Maciążek-Jurczyk, J. Równicka, W.W. Sulkowski, J. Mol. Struct. 924-926 (2009) 332-337. [doi: 10.1016/j.molstruc.2008.12.015]

[13] M. Varela, C. Cabezas, J.C. Lopez, J.L. Alonso, J. Phys. Chem. A 117 (2013) 13275-13278. [doi: 10.1021/jp404581z]

[14] J.G. Camilotti, A. Somer, G.F. Costa, M.A. Ribeiro, C. Bonardi, G.K. Cruz, S.L. Gómez, F.L. Beltrame, A.N. Medina, F. Sato, N.G.C. Astrath, A. Novatski, Spectrochim. Acta A 121 (2014) 719-723. [doi: 10.1016/j.saa.2013.11.099]

[15] H. Bahrami, H. Farrokhpour. Corona discharge ionization of paracetamol molecule: Peak assignment. Spectrochim. Acta A, 135 (2015) 646-651. [doi: 10.1016/j.saa.2014.07.064]

[16] M. Fujiwara, P.S. Chow, D.L. Ma, R.D. Braatz, Cryst. Growth Des. 2 (2002) 363-370. [doi: 10.1021/cg0200098]

[17] S.C. Barthe, M.A. Grover, R.W. Rousseau, Cryst. Growth Des. 8 (2008) 3316-3322. [doi: 10.1021/cg800232x]

[18] C.J. Brown, X. Ni, Cryst. Growth Des. 11 (2011) 719-725. [doi: 10.1021/cg1011988]

[19] V.M. Andre, M.F.da Piedade, M.T. Duarte, CrystEngComm 14 (2012) 5005-5014. [doi: 10.1039/C2CE25307K]

[20] J. Sibik, M.J. Sargent, M. Franklin, J.A. Zeitler, Mol. Pharmaceutics 11 (2014) 1326-1334. [doi: 10.1021/mp400768m]

[21] H. Jain, K.S. Khomane, A.K. Bansal, CrystEngComm, 16 (2014) 8471-8478. [doi: 10.1039/C4CE00878B]

[22] M.A. Alisi, M. Brufani, N. Cazzolla, F. Ceccacci, P. Dragone, M.F.G. Furlotti, B. Garofalo, A. La Bella, O. Lanzalunga, F. Leonelli, R.M. Bettolo, C. Maugeri, L.M. Migneco, V. Russo, Tetrahedron, 68 (2012) 10180-10187. [doi: 10.1016/j.tet.2012.09.098]

[23] R. van de Straat, G.J. Bijloo, N.P.E. Vermeulen, Biochem. Pharmac., 37 (1988) 3473-3476. [doi: 10.1016/0006-2952(88)90699-5]

[24] V. Onnis, C. Congiu, E. Björklund, F. Hempel, E. Söderström, C.J. Fowler, J. Med. Chem. 53 (2010) 2286-2298. [doi: 10.1021/jm901891p]

[25] J.G.M. Bessems, H.-D. Gaisser, J.M. Te Koppele, W.P. Van Bennekom, J.N.M. Commandeur, N.P.E. Vermeulen, Chem. Biol. Interact. 98 (1995) 237-250. [doi: 10.1016/0009-2797(95)03649-0]

[26] J.G.M. Bessems, L.L.P. Van Stee, J.N.M. Commandeur, E.J. Groot, N.P.E. Vermeulen, Toxicol. in Vitro 11 (1997) 9-19. [doi: 10.1016/S0887-2333(96)00066-5]

-22-

[27] M. Since, T. Freret, G. Nee, T. Terme, P. Vanelle, M. Boulouard, Eur. J. Med. Chem., 69 (2013) 728-734. [doi: 10.1016/j.ejmech.2013.08.041]

[28] R.V. Shchepin, W. Liu, H. Yin, I. Zagol-Ikapitte, T. Amin, B.-S. Jeong, L.J. Roberts, J.A. Oates, N.A. Porter, O. Boutaud, ACS Med. Chem. Lett. 4 (2013) 710-714. [doi: 10.1021/ml4000904]

[29] M.R. Yadav, D.M. Nimekar, A. Ananthakrishnan, P.S. Brahmkshatriya, S.T. Shirude, R. Giridhar, A. Parmar, R. Balaraman, Bioorgan. Med. Chem. 14 (2006) 8701-8706. [doi: 10.1016/j.bmc.2006.08.017]

[30] M.L. Barbosa, G.M. Melo, Y.K. da Silva, R.D.O. Lopes, E.T. de Souza, A.C. de Queiroz, S. Smaniotto, M.S. Alexandre-Moreira, E.J. Barreiro, L.M. Lima, Eur. J. Med. Chem. 44 (2009) 3612-3620. [doi: 10.1016/j.ejmech.2009.02.026]

[31] A. Ahmadi, M. Khalili, S. Ahmadian, N. Shahghobadi, B. Nahri-Niknafs, Pharm. Chem. J. 48 (2014) 109-115. [doi: 10.1007/s11094-014-1059-x]

[32] M. Gaba, D. Singh, S. Singh, V. Sharma, P. Gaba, Eur J Med Chem. 45 (2010) 2245-2249. [doi: 10.1016/j.ejmech.2010.01.067]

[33] R.F.W. Bader, Atoms in Molecules: A Quantum Theory, Oxford University Press, Oxford, 1990.

[34] R. Moreno-Fuquen, D.E. Quintero, F. Zuluaga, R.L.A. Haiduke, A.R. Kennedy, 2-Bromo-2-methyl-N-(4-nitrophenyl)propanamide, Acta Cryst. E67 (2011) o659. [doi: 10.1107/S1600536811005320]

[35] R. Moreno-Fuquen, D. E. Quintero, F. Zuluaga, A. R. Kennedy and R. H. De Almeida Santos, Acta Cryst. E67 (2011) o1543 [doi: 10.1107/S1600536811019337]

[36] C.R. Martins, L.C. Ducati, C.F. Tormena, R. Rittner, Spectrochim. Acta A 72 (2009) 1089-1096. [doi: 10.1016/j.saa.2009.01.002]

[37] R. Rittner, L.C. Ducati, C.F. Tormena, B.C. Fiorin, C.B. Braga, Spectrochim. Acta A 79 (2011) 1071-1076. [doi: 10.1016/j.saa.2011.04.021]

[38] R. Rittner, L.C. Ducati, C.F. Tormena, R.A. Cormanich, B.C. Fiorin, C.B. Braga, R.J. Abraham, Spectrochim. Acta A 103 (2013) 84-89. [doi: 10.1016/j.saa.2012.11.013]

[39] R.A. Cormanich, L.C. Ducati, C.F. Tormena, R. Rittner, Spectrochim. Acta A 123 (2014) 482-489. [doi: 10.1016/j.saa.2013.12.088]

[40] C.G. Oliveira, P.I.D.S. Maia, P.C. Souza, F.R. Pavan, C.Q.F. Leite, R.B. Viana, A.A. Batista, O.R. Nascimento, V.M. Deflon, J. Inorg. Biochem. 132 (2014) 21-29. [doi: 10.1016/j.jinorgbio.2013.10.011]

[41] F.C.A. Lima, R.B. Viana, T.T. da Silva, S.M.S.V. Wardell, A.P.N. do Filho, J.W.M. Carneiro, M. Comar Jr., A.B.F. da Silva, J. Mol. Model. 18 (2012) 3243-3253. [doi: 10.1007/s00894-011-1323-x]

[42] F.C.A. Lima, R.B. Viana, J.W.M. Carneiro, M. Comar Jr., A.B.F. da Silva, Struct. Chem. 23 (2012) 1539-1545. [doi: 10.1007/s11224-012-9950-0]

[43] Gaussian 09, Revision D.01, M. J. Frisch, G. W. Trucks, H. B. Schlegel, G. E. Scuseria, M. A. Robb, J. R. Cheeseman, G. Scalmani, V. Barone, B. Mennucci, G. A. Petersson, H. Nakatsuji, M. Caricato, X. Li, H. P. Hratchian, A. F. Izmaylov, J. Bloino, G. Zheng, J. L. Sonnenberg, M. Hada, M. Ehara, K. Toyota, R. Fukuda, J. Hasegawa, M. Ishida, T. Nakajima, Y. Honda, O. Kitao, H. Nakai, T. Vreven, J. A. Montgomery, Jr., J. E. Peralta, F. Ogliaro, M. Bearpark, J. J. Heyd, E. Brothers, K. N. Kudin, V. N. Staroverov, R. Kobayashi, J. Normand, K. Raghavachari, A. Rendell, J. C. Burant, S. S. Iyengar, J. Tomasi, M. Cossi, N. Rega, J. M. Millam, M. Klene, J. E. Knox, J. B. Cross, V. Bakken, C. Adamo, J. Jaramillo, R. Gomperts, R. E. Stratmann, O. Yazyev, A. J. Austin, R. Cammi, C. Pomelli, J. W. Ochterski, R. L. Martin, K. Morokuma, V. G. Zakrzewski, G. A. Voth, P. Salvador, J. J. Dannenberg, S. Dapprich, A. D. Daniels, Ö. Farkas, J. B. Foresman, J. V. Ortiz, J. Cioslowski, and D. J. Fox, Gaussian, Inc., Wallingford CT, 2009.

[44] J.P. Perdew, K. Burke, M. Ernzerhof, Phys. Rev. Lett. 77 (1996) 3865-3868. [doi: 10.1103/PhysRevLett.77.3865]

[45] C. Adamo, V. Barone, J. Chem. Phys. 110 (1999) 6158-6169. [doi: 10.1063/1.478522]

[46] M.J. Frisch, J.A. Pople, J.S. Binkley, J. Chem. Phys. 80 (1984) 3265-3269. [doi: 10.1063/1.447079]

[47] R. C. Binning Jr., L. A. Curtiss, J. Comp. Chem., 11 (1990) 1206-1216. [doi: 10.1002/jcc.540111013]

[48] A.L. Hickey, C.N. Rowley, J. Phys. Chem. A 118 (2014) 3678-3687. [doi: 10.1021/jp502475e]

[49] S. Andersson, M. Gruning, J. Phys. Chem. A 108 (2004) 7621-7636. [doi: 10.1021/jp040448c]

[50] L. Simon, J.M. Goodman, Org. Biomol. Chem. 9 (2011) 689-700. [doi: 10.1039/c0ob00477d]

[51] Y. Zhao, N. Gonzalez-Garcia, D.G. Truhlar, J. Phys. Chem. A 109 (2005) 2012-2018. [doi: 10.1021/jp045141s]

[52] C. Peng, H.B. Schlegel, Israel J. Chem. 33 (1993) 449-54. [doi: 10.1002/ijch.199300051]

[53] C. Peng, P.Y. Ayala, H.B. Schlegel, M.J. Frisch, J. Comp. Chem. 17 (1996) 49-56. [doi: 10.1002/(SICI)1096-987X(19960115)17:1<49::AID-JCC5>3.0.CO;2-0]

[54] H.P. Hratchian, H.B. Schlegel, J. Chem. Phys. 120 (2004) 9918-24. [doi: 10.1063/1.1724823]

[55] H.P. Hratchian, H.B. Schlegel, J. Chem. Theory Comput. 1 (2005) 61-69. [doi: 10.1021/ct0499783]

[56] Y. Zhao, N.E. Schultz, D.G. Truhlar, J. Chem. Theory and Comput. 2 (2006) 364-382. [doi: 10.1021/ct0502763]

[57] A.D. Boese, J.M.L. Martin, J. Chem. Phys. 121 (2004) 3405-3416. [doi: 10.1063/1.1774975]

-24-

[58] F. Yu, J. Comp. Chem. 33 (2012) 1347-1352. [doi: 10.1002/jcc.22963]

[59] Y. Zhao, D.G. Truhlar, Acc. Chem. Res. 41 (2008) 157-167. [doi: 10.1021/ar700111a]

[60] J. Cioslowski, J. Am. Chem. Soc. 111 (1989) 8333-8336. [doi: 10.1021/ja00204a001]

[61] A.E. Reed, R.B. Weinstock, F. Weinhold, J. Chem. Phys. 83 (1985) 735. [doi: 10.1063/1.449486]

[62] L.E. Chirlian, M.M. Francl, J. Comp. Chem. 8 (1987) 894-905. [doi: 10.1002/jcc.540080616]

[63] C.M. Breneman, K.B. Wiberg, J. Comp. Chem. 11 (1990) 361-73. [doi: 10.1002/jcc.540110311]

[64] U.C. Singh, P.A. Kollman, J. Comp. Chem. 5 (1984) 129-45. [doi: 10.1002/jcc.540050204]

[65] B.H. Besler, K.M. Merz Jr., P.A. Kollman, J. Comp. Chem. 11 (1990) 431-39. [doi: 10.1002/jcc.540110404]

[66] F.L. Hirshfeld, Theor. Chem. Acc., 44 (1977) 129-138. [doi: 10.1007/BF00549096]

[67] J.P. Ritchie, S.M. Bachrach, J. Comp. Chem. 8 (1987) 499-509. [doi: 10.1002/jcc.540080430]

[68] NBO 6.0. E.D. Glendening, J.K. Badenhoop, A.E. Reed, J.E. Carpenter, J.A. Bohmann, C.M. Morales, C.R. Landis, F. Weinhold (Theoretical Chemistry Institute, University of Wisconsin, Madison, WI, 2013) (http://nbo6.chem.wisc.edu/)

[69] AIMAll, Todd A. Keith, TK Gristmill Software, Overland Park KS, USA, 2011 (aim.tkgristmill.com).

[70] F. Martin, H. Zipse, J. Comp. Chem. 26 (2005) 97-105. [doi: 10.1002/jcc.20157]

[71] M.F. Lucas, M.C. Michelini, N. Russo, E. Sicilia, J. Chem. Theory Comput. 4 (2008) 397-403. [doi: 10.1021/ct700277w]

[72] R.B. Viana, A.B.F. da Silva, Polyhedron 89 (2015) 160-167. [doi: 10.1016/j.poly.2015.01.010]

[73] R.B. Viana, A.B.F da Silva, J. Mol. Model. 20 (2014) 2372. [doi: 10.1007/s00894-014-2372-8]

[74] R.B. Viana, A.R. Guimaraes, A.R. de Souza, A.B.F da Silva, J. Mol. Model. 20 (2014) 2074. [doi: 10.1007/s00894-014-2074-2]

[75] C.J. Cramer, Essentials of Computational Chemistry - Theories and Models, 2nd Edition, John Wiley & Sons, Chichester, England, 2004.

[76] M. Karelson, V.S. Lobanov, A.R. Katritzky, Chem. Rev. 96 (1996) 1027-1044. [doi: 10.1021/cr950202r]

[77] A. Arroio, K.H. Honorio, A.B.F da Silva, Quim. Nova 33 (2010) 694-699. [doi: 10.1590/S0100-40422010000300037]

[78] J.C. Gertrudes, V.G. Maltarollo, R.A. Silva, P.R. Oliveira, K.M. Honorio, A.B.F. da Silva, Curr. Med. Chem. 19 (2012) 4289-4297. [doi: 10.2174/092986712802884259]

[79] L.A. Curtiss, K. Raghavachari, P.C. Redfern, J.A. Pople, J. Chem. Phys. 106 (1997) 1063. [doi: 10.1063/1.473182]

[80] M.W. Chase, Jr., NIST-JANAF Thermochemical Tables, 4th ed., J. Phys. Chem. Ref. Data, Monograph, 9 (1998) 1.

[81] Moore, C. E. Atomic Energy Levels, Natl. Bur. Stand. U.S. Circ. No. 467 U.S. GPO, Washington, D.C., 1999.

[82] L. A. Curtiss, P. C. Redfern, K. Raghavachari, V. Rassolov, J. A. Pople, J. Chem. Phys. 110 (1999) 4703-4709. [doi: 10.1063/1.478385]

[83] L. Aydin, E. Sahan, Z. Onal, T. Ozpozan, Spectrochim. Acta A 129 (2014) 22-34. [doi: 10.1016/j.saa.2014.02.176]

[84] D. Sarigol, D. Yuksel, G. Okay, A.U. Baran, J. Mol. Struct. 1086 (20150 146-152. [doi: 10.1016/j.molstruc.2014.12.092]

[85] A. K. Ghose, A. Pritchett and G. M. Crippen, J. Comp. Chem. 9 (1988) 80-90. [doi:10.1002/jcc.540090111]

[86] HyperChem(TM) Professional 7.51, Hypercube, Inc., 1115 NW 4th Street, Gainesville, Florida 32601, USA

[87] R.D. Briciu, A. Kot-Wasik, J. Namiesnik, C. Sarbu, Acta Chromatogr. 21 (2009) 237-250. [doi: 10.1556/AChrom.21.2009.2.4]

[88] A. Hawryl, L. Popiolek, M. Dobosz, E. Pikula, M. Waksmundzka-Hajnos, Acta Chromatogr. 22 (2010) 37-55. [doi: 10.1556/AChrom.22.2010.1.3]

[89] C. Sarbu, R.D. Nascu-Briciu, D. Casoni, A. Kot-Wasik, A. Wasik, J. Namiesnik, J. Chromatogr. A 1266 (2012) 53-60. [doi:10.1016/j.chroma.2012.10.007]

[90] A.B. Denis, C.A. Diagone, A.M.G. Plepis, R.B. Viana, Spectrochim. Acta A 151 (2015) 908-915. [doi: 10.1016/j.saa.2015.07.040]

[91] I. Mayer, P. Salvador, Chem. Phys. Lett. 383 (2004) 368-375. [doi:10.1016/j.cplett.2003.11.048]

[92] K.B. Wiberg, Tetrahedron 24 (1968) 1083-1096. [doi: 10.1016/0040-4020(68)88057-3]

[93] X. Fradera, M.A. Austen, R.F.W. Bader, J. Phys. Chem. A, 103 (1999) 304-314. [doi: 10.1021/jp983362q]

[94] A.E. Reed, P.V.R. Schleyer, Inorg. Chem. 27 (1988) 3969-3987. [doi: 10.1021/ic00295a018]

[95] R.W. Bader, Chem. Rev. 91 (1991) 893-928. [doi: 10.1021/cr00005a013]

[96] D. Cremer, E. Kraka, Angew. Chem. Int. Ed. Engl. 23 (1984) 627-628. [doi: 10.1002/anie.198406271]

[97] Avogadro: an open-source molecular builder and visualization tool. Version 1.XX. <http://www.avogadro.openmolecules.net./>.

[98] G. Socrates, Infrared and Raman Characteristic Group Frequencies, 3rd ed., John Wiley & Sons, Ltd., Chichester, 2001.

[99] J. Mohan, Organic Spectroscopy, Principle and Applications, 2nd ed., New Age International (P) Limited Publishers, New Delhi, 2001.

[100] V. Krishnakumar, R. Mathammal, J. Raman Spectrosc. 40 (2009) 1104-1109. [doi: 10.1002/jrs.2236]

[101] S. Qiu, L. Liu, X. Jin, A. Zhang, K. Wu, L. Wang, Spectrochim. Acta A 77 (2010) 572-578. [doi: 10.1016/j.saa.2010.05.012]

[102] S. Qiu, X. Tan, K. Wu, A. Zhang, S. Han, L. Wang, Spectrochim. Acta A 76 (2010) 429-434. [doi: 10.1016/j.saa.2009.10.005]

[103] R.J. Xavier, E. Gobinath, Spectrochim. Acta A 97 (2012) 215-222. [doi: 10.1016/j.saa.2012.06.008]

[104] V. Krishnakumar, N. Jayamani, R. Mathammal, J. Raman Spectrosc. 40 (2009) 936-940. [doi: 10.1002/jrs.2203]

[105] M. Govindarajan, S. Periandy, K. Carthigayen, Spectrochim. Acta A 97 (2012) 411-422. [doi: 10.1016/j.saa.2012.06.028]

[106] S. Muthu, E.E. Porchelvi, Spectrochim. Acta A 115 (2013) 275-286. [doi: 10.1016/j.saa.2013.06.011]

[107] R.B. Viana, A.B.F. da Silva, A.S. Pimentel, Int. J. Mol. Sci. 13 (2012) 7980-7993. [doi: 10.3390/ijms13077980]

[108] R.B. Viana, A.B.F. da Silva, A.S. Pimentel, Adv. Phys. Chem. 2012 (2012) 903272. [doi: 10.1155/2012/903272]

[109] R.B. Viana, E.D.A. Santos, L.J. Valencia, R.M. Cavalcante, E.B. Costa, R. Moreno-Fuquen, A.B.F. da Silva. Spectrochim. Acta A 102 (2013) 386-392. [doi: 10.1016/j.saa.2012.09.094]

[110] C.Y. Panicker, H.T. Varghese, L. Ushakumari, T. Ertan, I. Yildiz, C.M. Granadeiro, H.I.S. Nogueira, Y.S. Mary, J. Raman Spectrosc. 41 (2010) 381-390. [doi: 10.1002/jrs.2471]

[111] N. Emir, M. Bilge, M. Tursun, G. Kesan, C. Parlak, Spectrochim. Acta A 127 (2014) 388-395. [doi: 10.1016/j.saa.2014.02.085]

[112] Y.S. Mary, C.Y. Panicker, H.T. Varghese, K. Raju, T.E. Bolelli, I. Yildiz, C.M. Granadeiro, H.I.S. Nogueira, J. Mol. Struct. 994 (2011) 223-231. [doi: 10.1016/j.molstruc.2011.03.022]

[113] T.M. Kolev, P. Angelov, Spectrochim. Acta A 69 (2008) 559-565. [doi: 10.1016/j.saa.2007.05.003]

[114] A.S. El-Shahawy, S.M. Ahmed, N.Kh. Sayed, Spectrochim. Acta A 66 (2007) 143-152. [doi: 10.1016/j.saa.2006.02.034]

Figure caption

Figure 1. In the left side is showed the 2-Bromo-2-methyl-N-(4-nitrophenyl)-propanamide (**n1**) and 2-Bromo-2-methyl-N-p-tolyl-propanamide (**c1**) optimized structures with PBE1PBE/6-31G(2df,2pd). In the right side is demonstrated the structural superposition of calculated (in red) crystallographic structures (in blue; from references 34 and 35) for each compound.

Figure 2. Frontier orbitals of 2-Bromo-2-methyl-N-(4-nitrophenyl)-propanamide (**n1**) and 2-Bromo-2-methyl-N-p-tolyl-propanamide (**c1**) predicted with PBE1PBE/6-31G(2df,2pd).

Figure 3. Relative stability (in kcal mol^{-1}) among the regioisomers involving the different positions of the functional groups in the phenyl ring of both paracetamol analogues by (PBE1PBE/6-31G(2df,2pd)), [M05-2X/6-311++G(d,p)] and {BMK/6-311++G(d,p)}. The electric dipole moment (μ) is in Debye.

Figure 4. Relative energetic profile (in kcal mol^{-1}) of the E/Z configuration change reaction and the keto/enol unimolecular rearrangement of both paracetamol analogues by (PBE1PBE/6-31G(2df,2pd)), [M05-2X/6-311++G(d,p)] and {BMK/6-311++G(d,p)}.

Figure 5. Molecular electrostatic potential of each isomer mapped with an isovalue of 0.0004 a.u. The right side view represents the front of the solid surface, while the left side view shows the back of the surface and displays the molecular disposition.

Figure 6. Molecular graphs of the isomers. Green points represent bond critical points (BCP) and red points indicate ring critical points (RCP) and blue points represent cage critical points (CCP)

Figure 7. KBr infrared spectrum of 2-Bromo-2-methyl-N-p-tolyl-propanamide (**c1**).

Figure 8. KBr infrared spectrum of 2-Bromo-2-methyl-N-(4-nitrophenyl)-propanamide (**n1**).

Table 1. The Gibbs free activation energy (ΔG^0, in kcal mol^{-1}), the rate constant (κ, in s^{-1}) and the half-lifetime (τ, in s) at 298.15K of each reaction by three different functionals

Property	c1 $\rightarrow$ c2		c2 $\rightarrow$ c3		n1 $\rightarrow$ n2		n2 $\rightarrow$ n3	
	Forward	Reverse	Forward	Reverse	Forward	Reverse	Forward	Reverse
ΔG^0 PBE1PBE	19.6	10.1	34.5	24.6	18.6	7.1	32.8	25.5
M05-2X	17.2	7.0	37.1	30.2	17.2	7.0	37.1	30.2
BMK	17.4	6.3	37.3	28.8	17.4	6.3	37.3	28.8
κ PBE1PBE	2.58×10^{-2}	2.65×10^5	3.30×10^{13}	6.26×10^{-6}	1.40×10^{-1}	3.92×10^7	6.01×10^{-12}	1.18×10^{-6}
M05-2X	1.46	4.92×10^7	4.14×10^{-15}	4.26×10^{-10}	1.46	4.92×10^7	4.14×10^{-15}	4.26×10^{-10}
BMK	1.07	1.58×10^8	3.0×10^{-15}	4.53×10^{-9}	1.07	1.56×10^8	3.0×10^{-15}	4.53×10^{-9}
τ PBE1PBE	38.82	3.77×10^{-6}	3.03×10^{12}	1.6×10^5	7.15	2.55×10^{-8}	1.66×10^{11}	8.44×10^5
M05-2X	0.69	2.03×10^{-8}	2.42×10^{14}	2.35×10^9	0.69	2.03×10^{-8}	2.42×10^{14}	2.35×10^9
BMK	0.94	6.41×10^{-9}	3.33×10^{14}	2.21×10^8	0.94	6.41×10^{-9}	3.33×10^{14}	2.21×10^8

* For the PBE1BE functional was used the 6-31G(2df,2pd) basis sets, while for M05-2X and BMK functionals were employed the 6-311++G(d,p) basis sets.

Table 2. The electric dipole moment (μ, in Debye), log P, surface area (in Å^2), volume (in Å^3), refractivity index, mean polarizability (α, in a.u.), relative steric energy (E_{steric}, in kcal mol^{-1}) and the relative electrostatic energy (E_{static}, in kcal mol^{-1})

Property	c1	c2	c3	n1	n2	n3
Log P	4.87	4.87	3.49	4.59	4.59	3.21
Surface area	422.89	406.33	407.24	426.83	411.42	411.35
Volume	674.81	660.3	664.17	680.73	666.83	670.1
Refractivity	36.69	36.69	33.72	38.08	38.08	35.11
μ	1.13	4.09	1.66	5.76	3.45	5.99
α	125.0	107.1	110.7	128.6	123.6	119.8
E_{steric}	0.0	-2.5	-4.4	0.0	1.0	-9.5
E_{static}	0.0	-5.3	11.4	0.0	1.4	0.8

Table 3. Several properties in bond critical points (BCPs) in the intramolecular interactions as the electronic charge density [$\rho(r)$] and its Laplacian [$\nabla^2\rho(r)$], total energy density [$H(r)$], ellipticity (ε), and the relationship between local potential energy and the local energy density [$|V(r)|/G(r)$]

c1	O-HC	Br-HN	**n1**	O-HC	Br-HN
$\rho(r)$	0.01851	0.02399	$\rho(r)$	0.01935	0.02460
$\nabla^2\rho(r)$	0.06481	0.06840	$\nabla^2\rho(r)$	0.06811	0.06867
$H(r)$	0.00123	0.00006	$H(r)$	0.00127	-0.00015
$|V(r)|/G(r)$	0.92	1.00	$|V(r)|/G(r)$	0.92	1.01
ε	0.17043	0.10745	ε	0.16798	0.09980

c2	CH-C	Br-HC	**n2**	CH-C	Br-HC
$\rho(r)$	0.01237	0.01132	$\rho(r)$	0.01295	0.01749
$\nabla^2\rho(r)$	0.04129	0.03397	$\nabla^2\rho(r)$	0.04258	0.04749
$H(r)$	0.00180	0.00139	$H(r)$	0.00163	0.00076
$|V(r)|/G(r)$	0.79	0.80	$|V(r)|/G(r)$	0.82	0.93
ε	0.34030	0.19311	ε	0.45732	0.01963

c3	CH-C	Br-HC	**n3**	CH-C	Br-HC
$\rho(r)$	0.01256	0.00673	$\rho(r)$	0.01203	0.00677
$\nabla^2\rho(r)$	0.04251	0.01953	$\nabla^2\rho(r)$	0.04165	0.01973
$H(r)$	0.00192	0.00095	$H(r)$	0.00192	0.00096
$|V(r)|/G(r)$	0.78	0.76	$|V(r)|/G(r)$	0.77	0.76
ε	1.18391	0.18120	ε	0.89458	0.18895
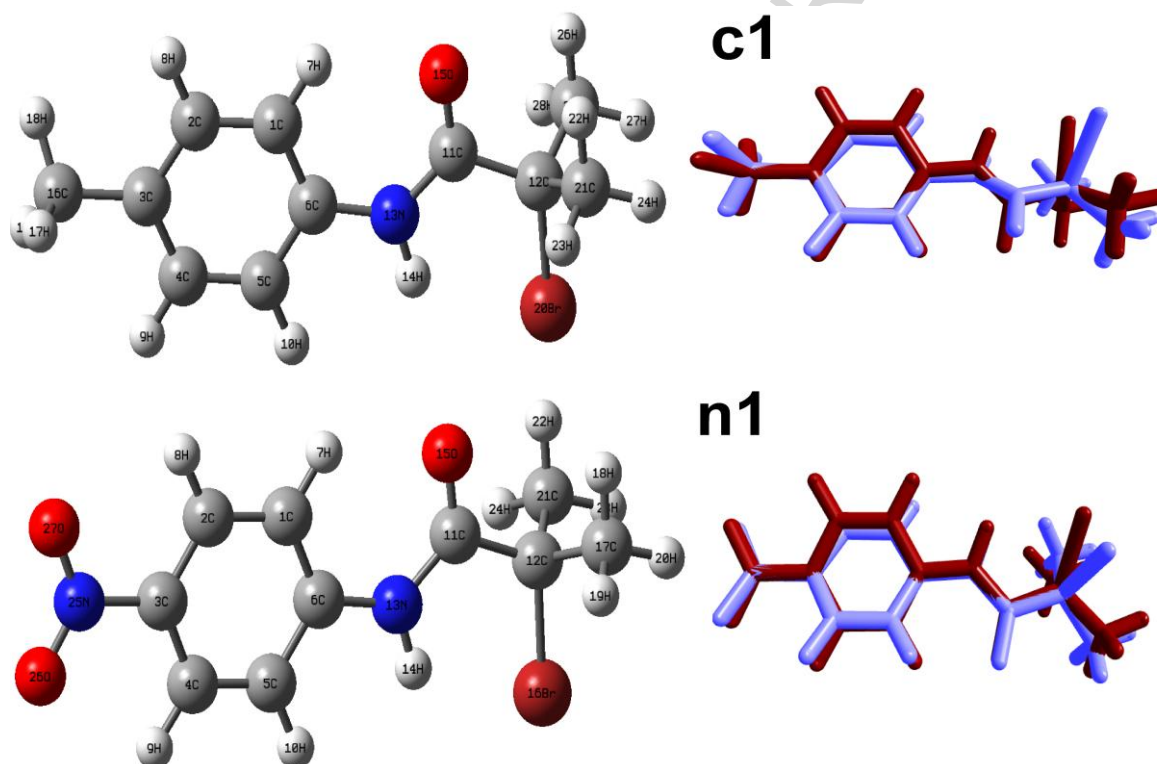
Figure 1.

LUMO
(-0.2 eV)

c1

LUMO
(0.1 eV)

Paracetamol

LUMO
(-2.1 eV)

n1

HOMO
(-6.2 eV)

HOMO
(-5.7 eV)

HOMO
(-7.1 eV)

Figure 2.

A
(0.0) / μ= 1.13
[0.0] / μ= 1.11
{0.0} / μ= 1.20

B
(2.6) / μ= 1.03
[0.6] / μ= 1.32
{2.1} / μ= 1.17

C
(-0.2) / μ= 0.78
[-0.3] / μ= 0.63
{-0.2} / μ= 0.76

D
(-0.2) / μ= 1.39
[-0.2] / μ= 1.38
{-0.2} / μ= 1.50

E
(0.3) / μ= 1.51
[-0.2] / μ= 1.50
{0.5} / μ= 1.64

A
(0.0) / μ= 5.76
[0.0] / μ= 6.19
{0.0} / μ= 6.55

B
(7.9) / μ= 3.95
[5.5] / μ= 4.22
{7.0} / μ= 4.46

C
(1.5) / μ= 5.55
[1.6] / μ= 6.04
{1.5} / μ= 6.34

D
(1.5) / μ= 2.63
[2.5] / μ= 2.72
{1.7} / μ= 2.91

E
(1.0) / μ= 4.04
[1.1] / μ= 4.59
{0.7} / μ= 4.73

Figure 3.

c1 (0.0)
    [0.0]
    {0.0}

TS1c | (19.0)
       [15.7]
       {15.8}

c2 (9.7)
    [9.6]
    {10.5}

TS2c | (43.5)
       [46.6]
       {47.2}

c3 (19.4)
    [15.9]
    {18.3}

n1 (0.0)
    [0.0]
    {0.0}

TS1n | (17.8)
       [15.7]
       {15.8}

n2 (11.0)
    [9.6]
    {10.5}

TS2n | (43.6)
       [46.6]
       {47.2}

n3 (18.4)
    [15.9]
    {18.3}
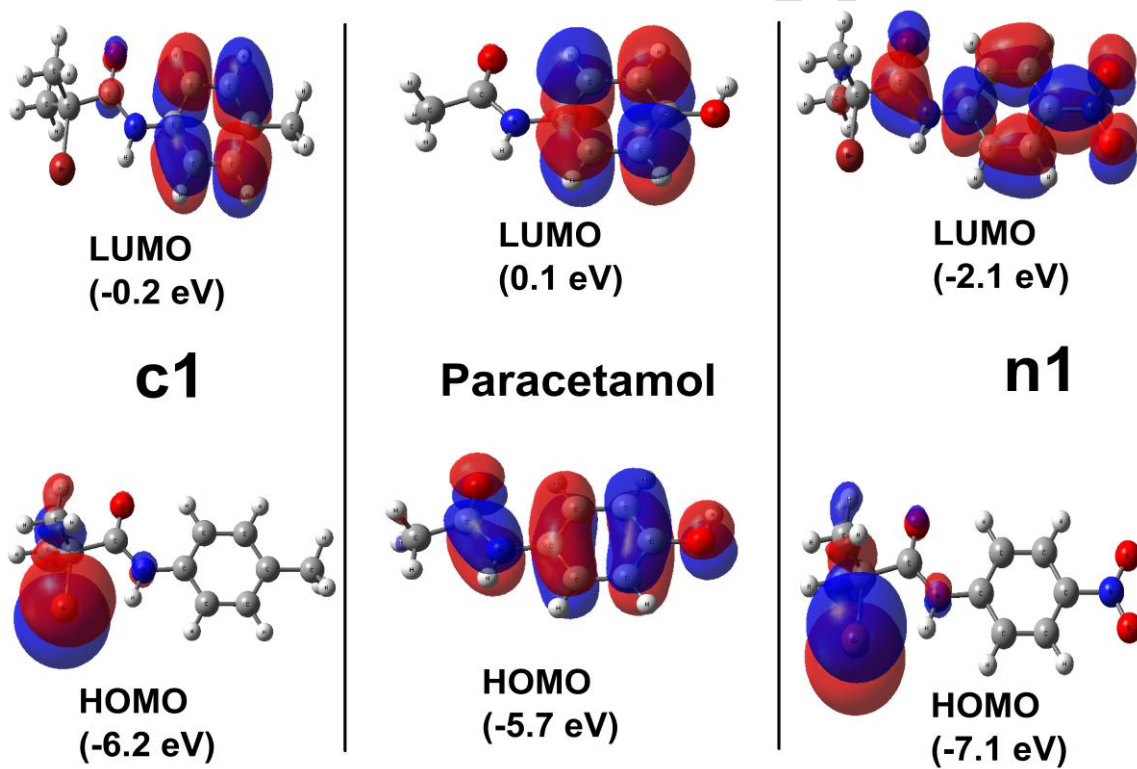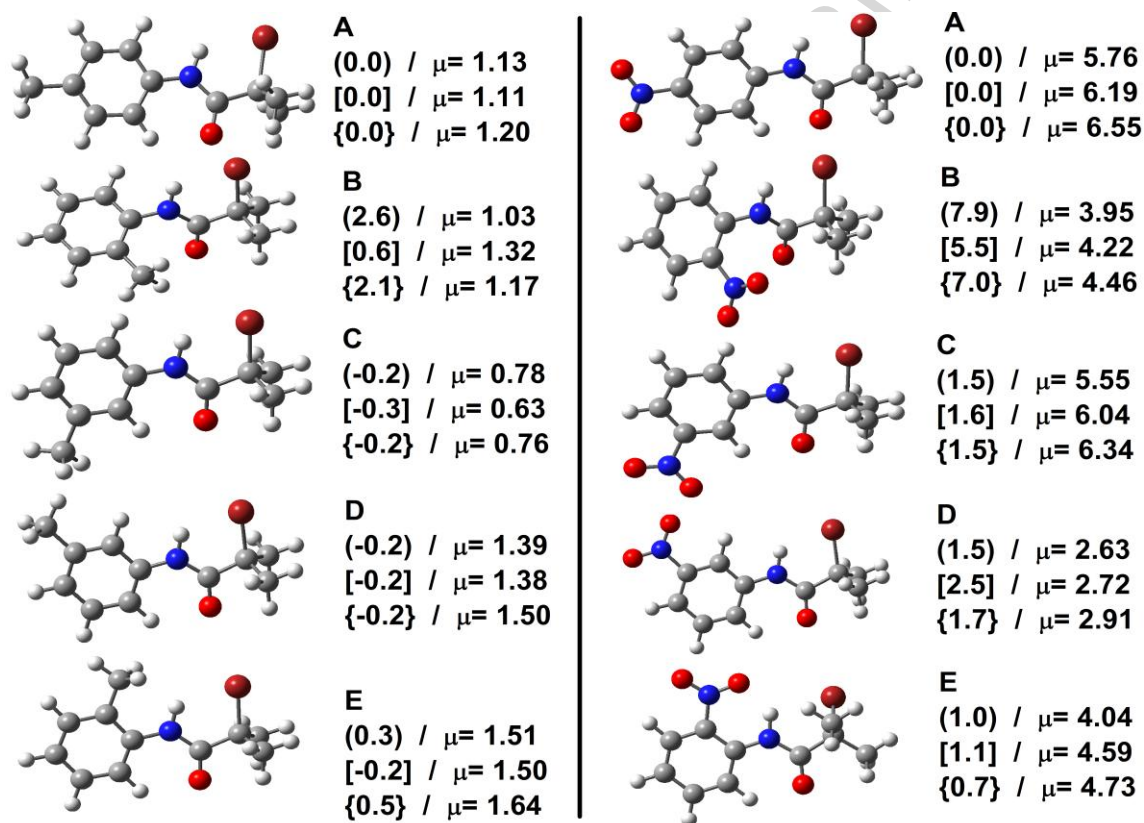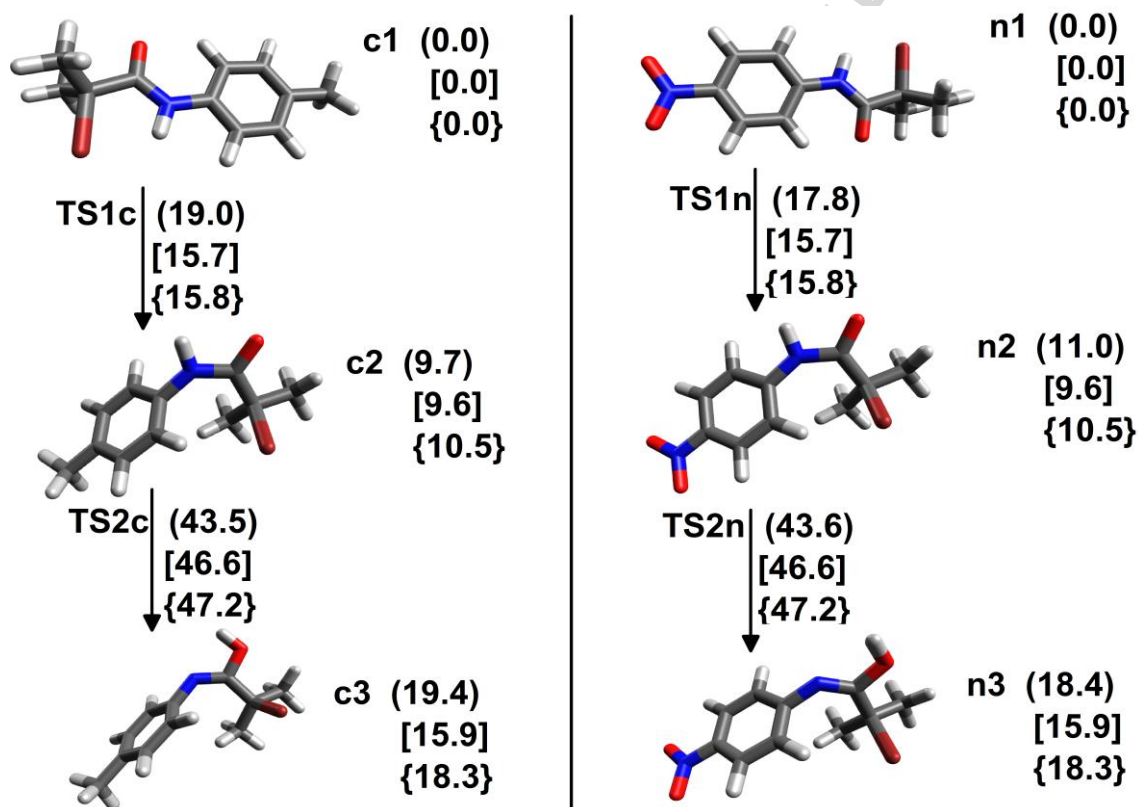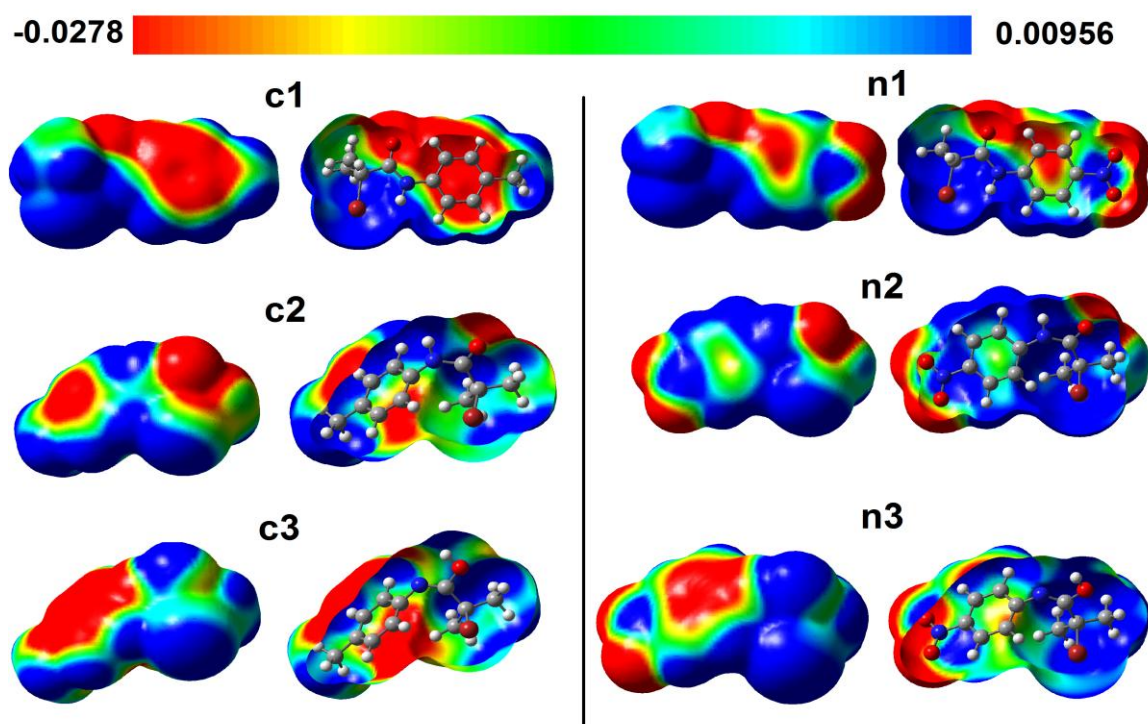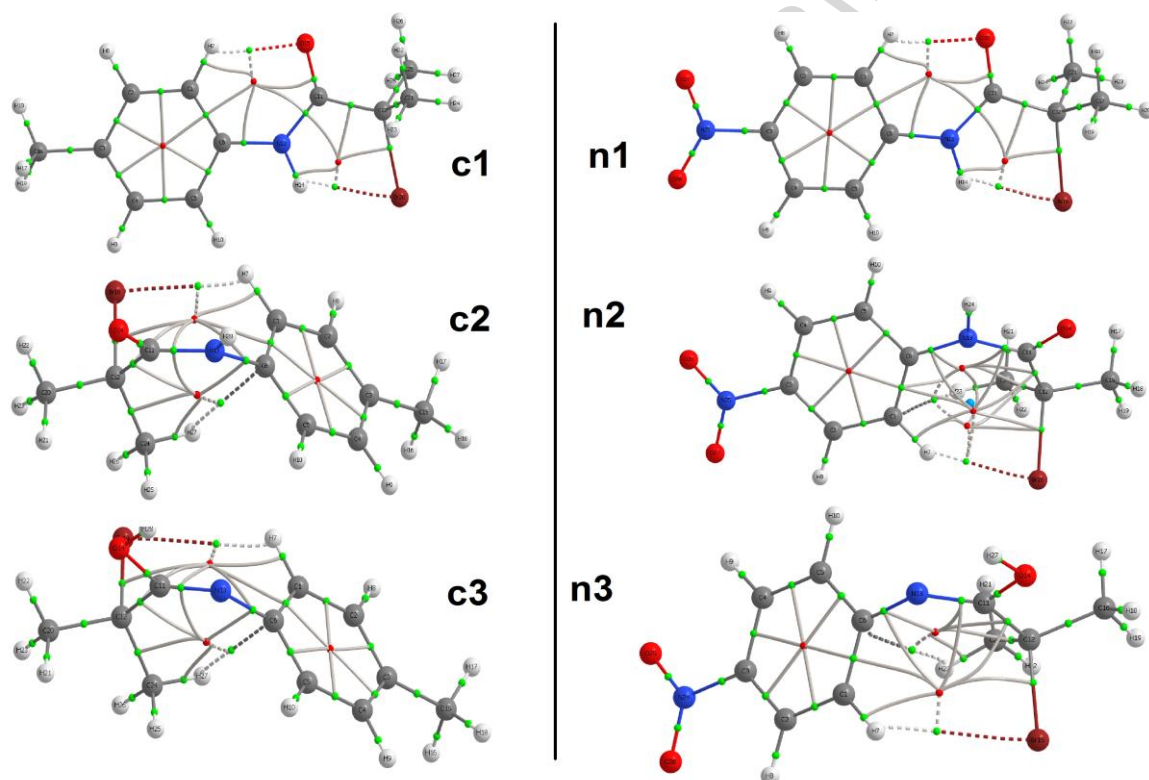
Figure 4.
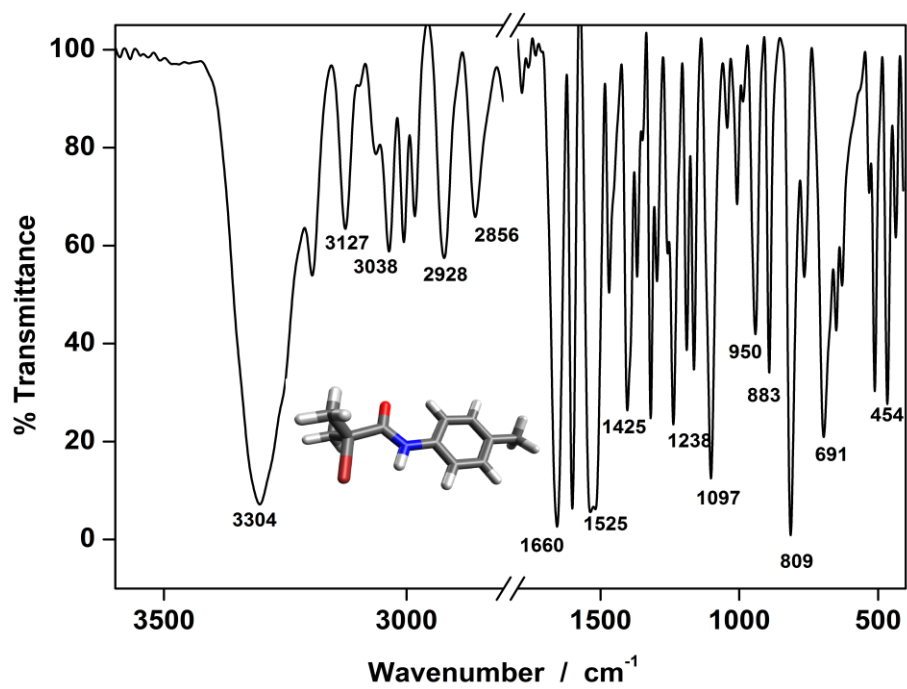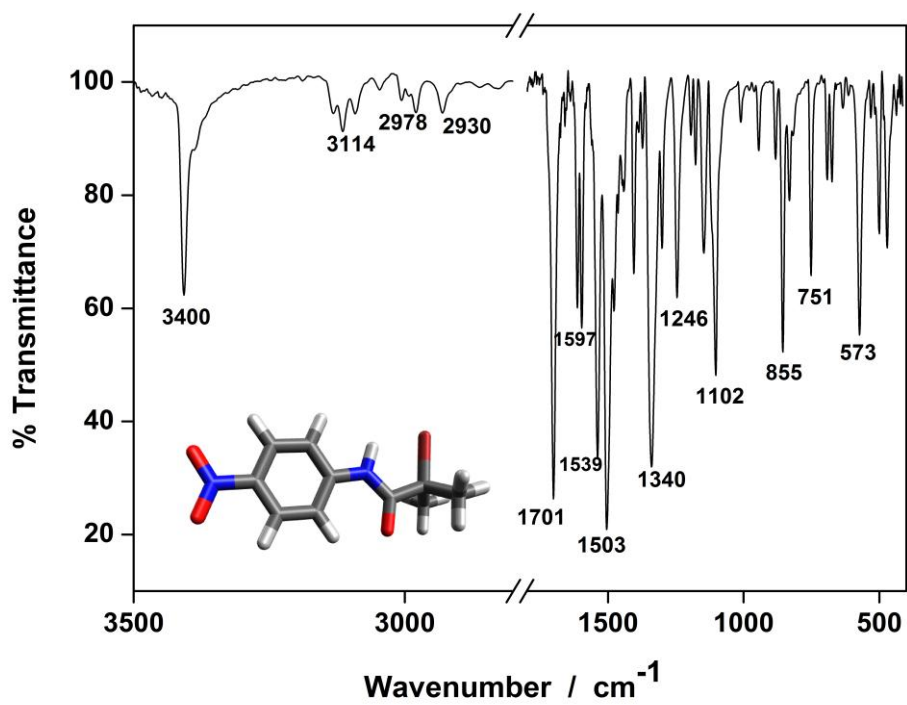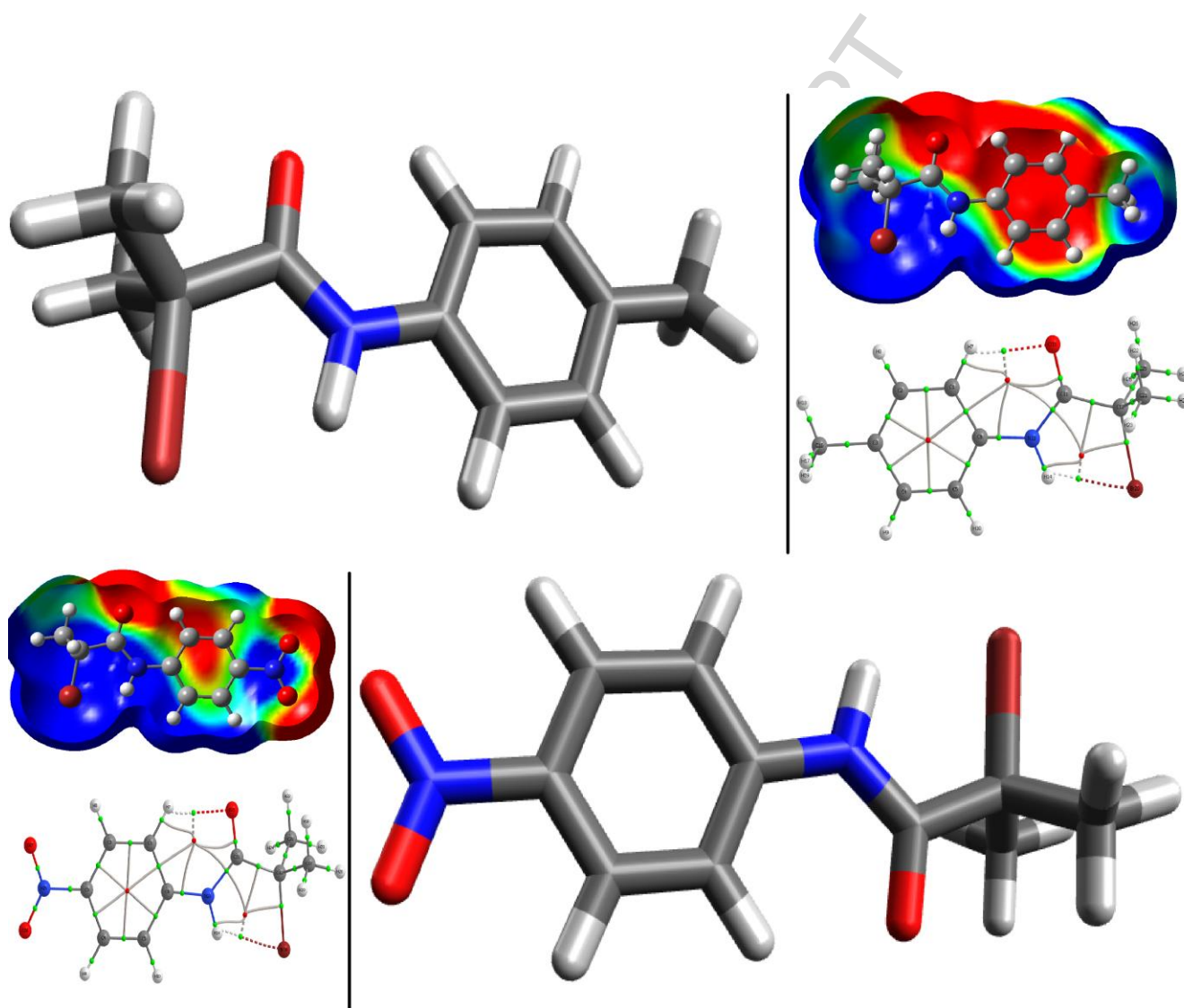
Figure 5.

Figure 6.

Figure 7.

Figure 8.

Graphical abstract

-39-

Highlights

- FT-IR of 2-bromo-2-methyl-N-(4-nitrophenyl)-propanamide
- FT-IR of 2-bromo-2-methyl-N-p-tolyl-propanamide
- Several properties: Log P, surface area, dipole moment, electrostatic potential
- Population methods: Chelp, ChelpG, NPA, QTAIM, Mulliken, Lowdin, MK, GAPT, Hirshfeld
- Heat of formation using the G3MP2 method